CHALMERS
FINITE ELEMENT CENTER

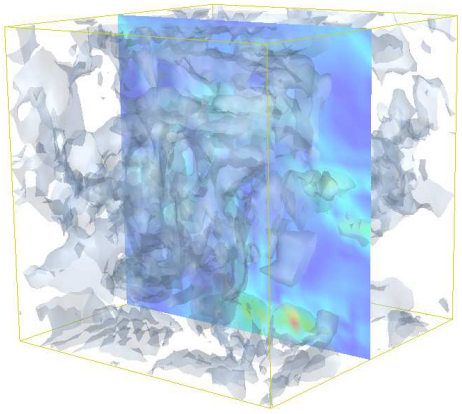

PREPRINT 2002–09

Adaptive multiscale computational modeling of complex incompressible fluid flow

Johan Hoffman and Claes Johnson

Chalmers Finite Element Center
CHALMERS UNIVERSITY OF TECHNOLOGY
Göteborg Sweden 2002

CHALMERS FINITE ELEMENT CENTER

Preprint 2002–09

Adaptive multiscale computational modeling of complex incompressible fluid flow

Johan Hoffman and Claes Johnson

CHALMERS

Chalmers Finite Element Center
Chalmers University of Technology
SE–412 96 Göteborg Sweden
Göteborg, May 2002

Adaptive multiscale computational modeling of complex incompressible fluid flow
Johan Hoffman and Claes Johnson
NO 2002–09
ISSN 1404–4382

Chalmers Finite Element Center
Chalmers University of Technology
SE–412 96 Göteborg
Sweden
Telephone: +46 (0)31 772 1000
Fax: +46 (0)31 772 3595
www.phi.chalmers.se

Printed in Sweden
Chalmers University of Technology
Göteborg, Sweden 2002

ADAPTIVE MULTISCALE COMPUTATIONAL MODELING OF COMPLEX INCOMPRESSIBLE FLUID FLOW

JOHAN HOFFMAN AND CLAES JOHNSON

ABSTRACT. We consider the problem of computational solution of the 3d Navier-Stokes equations in the case of complex non-stationary solutions with subgrid scales. We present adaptive finite element methods based on a posteriori error estimation in different norms of the discretization error and the modeling error from unresolved subgrid scales. The a posteriori error estimates involve discretization residuals and estimates of modeling residuals by extrapolation, combined with multiplicative weights computed by solving linearized dual problems. The a posteriori error estimates indicate computability of different quantities and may be used to select optimal meshes as well as the best of avaliable subgrid models. We present examples including transition to turbulence in shear flow, where we estimate the modeling error to be of the same order as the discretization error, and local quantities to be more demanding to compute than global. We also present results using different subgrid models.

1. INTRODUCTION

Error control in Computational Fluid Dynamics CFD has long been restricted to different forms of *ad hoc* approaches. In the last couple of years, new possibilities of quantitative error control and adaptive computational modeling have been opened by *adaptive finite element methods* based on *a posteriori error estimates* in the work by Johnson and Rannacher with co-workers [2]. Applications to laminar flows have been made with considerable success, see e.g. [11] and [18]. The discretization uses the general space-time Galerkin least squares stabilized finite element method, developed by Johnson and Hughes with coworkers, referred to as the General Galerkin G^2-method. This method includes the *streamline diffusion method* on Eulerian space-time meshes, the *characteristic Galerkin method* on Lagrangian space-time meshes with orientation along particle trajectories, and *Arbitrary Lagrangian-Eulerian ALE methods* with different mesh orientation. The G^2-method constitutes a general flexible methodology for the discretization of the incompressible and compressible Navier-Stokes equations applicable to a great variety of flow problems from creeping viscous flow to slightly viscous flow, including free or moving boundaries.

In [13] we extend the G^2-method to turbulent incompressible flow. To computationally resolve all scales in a *Direct numerical simulation* DNS may be possible for Reynolds

Date: May 3, 2002.

Key words and phrases. adaptivity, turbulence, subgrid modeling, a posteriori error estimation, modeling error.

Department of Computational Mathematics, Chalmers University of Technology, SE–412 96 Göteborg, Sweden, *email*: hoffman@math.chalmers.se, claes@math.chalmers.se .

numbers Re of the order up to 1000, while Re larger than say 100.000 is beyond present computational power. In typical applications in aero- and hydrodynamics we may have $Re = 10^6$ or larger. In these cases turbulence modeling is needed to account for unresolved subgrid scales on the computationally resolved scales. Turbulence modeling is one of classical physics outstanding open problems where today computational methods open new possibilities.

The a posteriori error estimates take into consideration both the numerical errors from discretization and the modeling errors from unresolved subgrid scales, and bound the total error in terms of an integral in space-time of a discretization residual times a dual weight, and a modeling residual times a dual weight. The dual weight is obtained by solving an associated linearized dual problem, and contains information about error propagation in space-time. If we use a subgrid model in the computation, the subgrid modeling error is included in the a posteriori error estimates, which opens the possibility of comparing the error using different subgrid models. Altogether the a posteriori error estimates open the possibility of adaptively choosing both an optimal mesh and an optimal subgrid model. We present computations of transition to turbulence in Couette flow, investigated in [12], with estimation of both the discretization error and the modeling error.

We emphasize that the error estimation depends on the computational goal: a pointwise quantity, a global measure of the error, or some local average of the solution, such as the temporal average of the drag force, for example. Through studies of the solution of the dual problem we find that, in a turbulent flow, a local quantity is more computationally demanding than a global.

2. Adaptive finite element methods for turbulent flow

The incompressible Navier-Stokes equations expressing conservation of momentum and incompressibility of a unit density constant temperature Newtonian fluid with constant kinematic viscosity $\nu > 0$ enclosed in a volume Ω in $\mathbb{R}^3$, take the form: Find (u, p) such that

$$\begin{aligned} \dot{u} + (u \cdot \nabla)u - \nu\Delta u + \nabla p &= f && \text{in } \Omega \times I, \\ \operatorname{div} u &= 0 && \text{in } \Omega \times I, \\ u &= w && \text{on } \partial\Omega \times I, \\ u(\cdot, 0) &= u^0 && \text{in } \Omega, \end{aligned} \tag{2.1}$$

where $u(x,t) = (u_i(x,t))$ is the *velocity* vector and $p(x,t)$ the *pressure* of the fluid at (x,t), and f, w, u^0, $I = (0,T)$, is a given driving force, Dirichlet boundary data, initial data and time interval, respectively. The quantity $\nu\Delta u - \nabla p$ represents the total fluid force, and may alternatively be expressed as

$$\nu\Delta u - \nabla p = \operatorname{div}\sigma(u,p), \tag{2.2}$$

where $\sigma(u,p) = (\sigma_{ij}(u,p))$ is the *stress tensor*, with components $\sigma_{ij}(u,p) = 2\nu\epsilon_{ij}(u) - p\delta_{ij}$, composed of the *stress deviatoric* $2\nu\epsilon_{ij}(u)$ with zero trace and an isotropic pressure: here $\epsilon_{ij}(u) = (u_{i,j}+u_{j,i})/2$ is the *strain tensor*, with $u_{i,j} = \partial u_i/\partial x_j$, and δ_{ij} is the usual Kronecker delta, the indices i and j ranging from 1 to 3. We assume that (2.1) is normalized so that

the reference velocity and typical length scale are both equal to one. The Reynolds number Re is then equal to ν^{-1}. Of course, the specification of the length scale may not be very obvious and thus the Reynolds number may not have a very precise quantitative meaning.

2.1. **The averaged Navier-Stokes equations.** In a turbulent flow we may not be able to resolve all spatial and temporal scales of the velocity u computationally. We may instead aim at computing a *running average* u^h of u on a scale h, defined by

$$u^h(x,t) = \frac{1}{h^4}\int_{Q_h}\int_{-h/2}^{h/2} u(x+y,t+s)\; dy\; ds, \tag{2.3}$$

where h is a constant parameter and $Q_h = \{y \in \mathbb{R}^3 : |y_i| \leq h/2\}$. We note that this operator commutes with space and time differentiation, and we now seek equations for u^h. If we take the running average of the equations (2.1), with suitable constructions near the boundary $\partial\Omega$, we obtain

$$\begin{aligned} \dot{u}^h + (u^h\cdot\nabla)u^h - \nu\Delta u^h + \nabla p^h + F_h(u) &= f && \text{in } \Omega\times I,\\ \operatorname{div} u^h &= 0 && \text{in } \Omega\times I,\\ u^h &= w && \text{on } \partial\Omega\times I,\\ u^h(\cdot,0) &= u^0 && \text{in } \Omega, \end{aligned} \tag{2.4}$$

where $F_h(u) = \operatorname{div}\,\tau^h(u)$, and $\tau_{ij}^h(u) = (u_iu_j)^h - u_i^hu_j^h$ is the *Reynolds stress tensor*. Alternatively, we may restrict u^h to denote pure spatial averaging. This procedure of averaging the Navier-Stokes equations over a certain spatial scale is referred to as a *Large eddy simulation* LES, see [5] for details. The crucial problem of LES is how to model $F_h(u)$ in terms of u^h in a subgrid model $\hat{F}_h(u^h)$, or $\tau^h(u)$ in a model $\hat{\tau}_h(u^h)$. In the rest of this paper we will let u^h be a spatial average only, defined by

$$u^h(x,t) = \frac{1}{h^3}\int_{Q_h} u(x+y,t)\; dy. \tag{2.5}$$

The difference of considering the case when we have u^h defined by (2.3) consist only in a reinterpretation of $\tau^h(u)$.

2.2. **Subgrid modeling.** There is a multitude of different subgrid models that correspond to different assumptions on the form of the Reynolds stresses, and we may formulate a "general" subgrid model on the form

$$\hat{\tau}_{ij}^h - \frac{1}{3}\hat{\tau}_{kk}^h = \check{\tau}_{ij}^h(u^h) + \check{\nu}_{ij}\epsilon_{ij}(u^h), \tag{2.6}$$

with an algebraic part and a viscous part, that contains several of the most commonly used models. We note that when we apply the trace-free form of the model (2.6), the isotropic part is absorbed into the pressure term, leading to a redefinition of the pressure, see [15].

The simplest, and most commonly used, subgrid models are the *eddy viscosity* models, where the effect of the Reynolds stresses is modeled as an extra viscosity, and corresponds

to $\check{\tau}_{ij}^h = 0$ and $\check{\nu}_{ij} = \nu_T$ in (2.6). The classical eddy viscosity model is the Smagorinsky model with

$$\nu_T = (C_S h)^2 |\epsilon(u^h)|, \tag{2.7}$$

where C_S is the Smagorinsky constant, commonly set to $0.1 - 0.2$. The eddy viscosity models are considered too dissipative, and they are unable to predict *backscatter*.

In general, the resolved scales are assumed to lie in the so called *inertial range*, which refers to a range of scales for which the energy spectrum has a simple power law behaviour, corresponding to *scale similarity*. Different types of scale similarity assumptions on the Reynolds stresses have been used to motivate various types of subgrid models. For example, in the *dynamic procedure* the parameters in a particular model are determined by comparing resolved Reynolds stresses on different scales, and in *scale similarity models* the assumption is that the exact Reynolds stresses are proportional to the resolved Reynolds stresses, possibly on coarser scales.

The concept of a dynamic model, first introduced by Germano [6], is not a subgrid model in itself, but rather a procedure that can be applied to different subgrid models, where the parameters in a particular model are determined by comparing resolved Reynolds stresses on different scales. If applied to the Smagorinsky model, for example, it corresponds to replacing the constant C_S by a function $C_S = C_S(x,t)$, which is determined by the dynamic procedure.

Scale similarity models, first introduced by Bardina [1], corresponds to $\check{\nu}_{ij} = 0$ in (2.6), and takes the form

$$\check{\tau}_{ij}^h(u^h) = \tau_{ij}^h(u^h) = (u_i^h u_j^h)^h - (u_i^h)^h (u_j^h)^h. \tag{2.8}$$

Variants of this type of models have been suggested by e.g. Liu [16], where the Reynolds stresses on the computational scale h are assumed to be proportional to Reynolds stresses of the resolved field on a coarser scale H:

$$\check{\tau}_{ij}^h(u^h) = C_L \tau_{ij}^H(u^h) = C_L((u_i^h u_j^h)^H - (u_i^h)^H (u_j^h)^H). \tag{2.9}$$

There are also dynamic variants of the scale similarity models, where C_L is determined by a dynamic procedure. The scale similarity models can predict backscatter, but are considered not to be dissipative enough.

Since the scale similarity models are considered not to be dissipative enough, they are often combined with an eddy viscosity model. This *mixed models* takes the form of (2.6), with $\check{\nu}_{ij} = \nu_T$ and $\check{\tau}_{ij}^h(u^h)$ being a scale similarity model. There are also dynamic variants where the parameters of both the eddy viscosity part and the scale similarity part are determined dynamically.

Among the subgrid models not mentioned above, we note the *Variational multiscale method* by Hughes [14], where an eddy viscosity model acts only on the finest resolved scales. There are *Fractal models*, see e.g. Scotti & Meneveau [19], that are based on fractal interpolation of the velocity field for a direct evaluation of the Reynolds stresses, and also models based on *homogenization* have been used, see e.g. [4].

2.3. **Scale similarity of turbulent solutions.** Turbulent flow show some features of scale similarity, which is expressed in the *Kolmogorov* 5/3-*law* [4], corresponding to Hölder continuity of the velocities with exponent 1/3. This gives some hope for scale similarity models, but features of coherent structures also present in turbulent flow pose challenges. In Section 4.1 we investigate the scale similarity with respect to a Haar MRA of a computed solution in a turbulent shear flow.

To motivate Hölder continuity of the velocities with exponent 1/3 we may argue as follows: If l is the smallest scale present in the flow and v is the corresponding velocity amplitude, then we should have $vl \sim \nu$ (local Reynolds number ~ 1) and $\nu(v^2/l^2) \sim 1$ (turbulent dissipation on the smallest scale), which gives $v^3 \sim l$, that is Hölder continuity with exponent 1/3 on the smallest scale, and by scale similarity we should have the same exponent also on coarser scales.

2.4. **The General Galerkin G^2-method for laminar flow.** In [11] we presented the general space-time Galerkin least squares stabilized finite element method, referred to as the General Galerkin G^2-method, for the incompressible Navier-Stokes equations (2.1). The least-squares stabilizations present in the G^2-method, take care of the two main difficulties traditionally met in the discretization of the incompressible Navier-Stokes equations, namely (i) instabilities from Eulerian discretization of convection terms, and (ii) pressure instabilities in equal order interpolation of velocity and pressure.

Let $0 = t_0 < t_1 < ... < t_N = T$ be a sequence of discrete time steps with associated time intervals $I_n = (t_{n-1}, t_n]$ of length $k_n = t_n - t_{n-1}$ and space-time slabs $S_n = \Omega \times I_n$, and let $W_n \subset H^1(\Omega)$ be a finite element space consisting of continuous piecewise polynomials of degree p on a mesh $\mathcal{T}_n = \{K\}$ of mesh size $h_n(x)$ with W_{0n} the functions in W_n vanishing on Γ. $H^1(\Omega)$ is the Hilbert space of Lebesgue square integrable functions with Lebesgue square integrable first order partial derivatives. To define the G^2-method for (2.1) with homogeneuos Dirichlet boundary conditions for the velocity ($w = 0$), let for a given velocity field β on $S_n = \Omega \times I_n$ vanishing on $\Gamma \times I_n$, the particle paths $x(\bar{x}, \bar{t})$ be defined by

$$\frac{dx}{d\bar{t}} = \beta(x, \bar{t}) \quad \bar{t} \in I_n, \quad \text{and} \quad x(\bar{x}, t_n) = \bar{x}, \quad \bar{x} \in \Omega, \tag{2.10}$$

and introduce the corresponding mapping $F_n^\beta : S_n \to S_n$ defined by $(x, t) = F_n^\beta(\bar{x}, \bar{t}) = (x(\bar{x}, \bar{t}), \bar{t})$, where $x = x(\bar{x}, \bar{t})$ satisfies (2.10). Define for a given $q \geq 0$, the spaces

$$\bar{V}_n^\beta = \{\bar{v} \in H^1(S_n)^3 : \bar{v}(\bar{x}, \bar{t}) = \sum_{j=0}^{q} (\bar{t} - t_n)^j U_j(\bar{x}),\ U_j \in [W_{0n}]^3\},$$

$$\bar{Q}_n^\beta = \{\bar{q} \in H^1(S_n) : \bar{q}(\bar{x}, \bar{t}) = \sum_{j=0}^{q} (\bar{t}_n - t_n)^j q_j(\bar{x}),\ q_j \in W_n\},$$

together with their analogs in (x, t)-coordinates: $V_n^\beta = \{v : \bar{v} \in \bar{V}_n^\beta\}$, $Q_n^\beta = \{q : \bar{q} \in \bar{Q}_n^\beta\}$, where $v(x, t) = \bar{v}(\bar{x}, \bar{t})$ and $q(x, t) = \bar{q}(\bar{x}, \bar{t})$. Defining finally $V^\beta \times Q^\beta = \prod_n V_n^\beta \times Q_n^\beta$, we can now formulate the G^2-method as follows: Find $(U, P) \in V^\beta \times Q^\beta$, such that for

$n = 1, 2, ..., N$,

$$
\begin{aligned}
&(\dot{U} + (U \cdot \nabla)U, v)_n - (P, \operatorname{div} v)_n + (q, \operatorname{div} U)_n + (2\nu\epsilon(U), \epsilon(v))_n \\
&+ (\delta_1 a(U; U, P), a(U; v, q))_n + (\delta_2 \operatorname{div} U, \operatorname{div} v)_n + ([U^{n-1}], v_+^{n-1}) \\
&= (f, v + \delta_1 a(U; v, q))_n \quad \forall (v, q) \in V_n^\beta \times Q_n^\beta,
\end{aligned} \tag{2.11}
$$

where $a(w; v, q) = D_{w,t}v + \nabla q - \nu\Delta v$ with the Laplacian defined elementwise, $\delta_1 = \frac{1}{2}(k_n^{-2} + |U|^2 h_n^{-2})^{-1/2}$ in the convection-dominated case $\nu < Uh_n$ and $\delta_1 = \kappa_1 h^2$ otherwise, $\delta_2 = \kappa_2 h$ if $\nu < Uh_n$ and $\delta_2 = \kappa_2 h^2$ otherwise, with κ_1 and κ_2 positive constants of unit size, and

$$
(v, w)_n = \int_{I_n} (v, w) dt, \quad (v, w) = \sum_{K \in \mathcal{T}_n} \int_K v \cdot w \, dx,
$$

$$
(\epsilon(v), \epsilon(w)) = \sum_{i,j=1}^{3} (\epsilon_{ij}(v), \epsilon_{ij}(w)).
$$

Further, $[v^n] = v_+^n - v_-^n$ is the jump across the time level t_n with $v_\pm^n$ the limit from $t > t_n / t < t_n$. In the Eulerian *streamline diffusion method* we choose $\beta = 0$, which means that the mesh does not move in time. The *characteristic Galerkin method* is obtained by choosing $\beta = U$ (and then $\delta_1 = \kappa_1 h^2$), which means that the mesh moves with the fluid particles. We may also choose β differently which gives various versions of ALE-methods, with the mesh and particle velocity being (partly) different; for example we may move the mesh with the particle velocity at a free boundary, while allowing the mesh to move differently inside the domain.

The variational formulation (2.11) with $\delta_1 = \delta_2 = 0$ is obtained by multiplying the momentum equation by v, integrating over S_n including integration by parts, and adding the incompressibility equation multiplied by q and integrating over S_n. Choosing δ_1 and δ_2 positive as indicated introduces stabilizing least-squares terms. Note that the viscous term $(2\nu\epsilon(U), \epsilon(v))_n$ may alternatively occur in the form $(\nu\nabla U, \nabla v)_n = \sum_{i=1}^3 (\nu\nabla U_i, \nabla v_i)_n$. In the case of Dirichlet boundary conditions the corresponding variational formulations are equivalent, but not so in the case of Neumann boundary conditions, see [11].

In extreme situations, we may add residual dependent *shock-capturing artificial viscosity*, replacing ν by $\tilde{\nu} = \max(\nu, \kappa_3 |R(U, P)| h^2)$, where $R(U, P) = \sum_{i=1}^4 R_i(U, P)$ with

$$
\begin{aligned}
R_1(U, P) &= |\dot{U} + U \cdot \nabla U + \nabla P - f - \nu\Delta U|, \\
R_2(U, P) &= \nu D_2(U), \\
R_3(U, P) &= |[U^{n-1}]|/k_n \quad \text{on } S_n, \\
R_4(U, P) &= |\operatorname{div} U|,
\end{aligned} \tag{2.12}
$$

where

$$
D_2(U)(x, t) = \max_{y \in \partial K} (h_n(x))^{-1} |[\frac{\partial U}{\partial n}(y, t)]|, \tag{2.13}
$$

for $x \in K$, with $[\cdot]$ the jump across the element edge ∂K, and κ_3 is a positive constant of unit size. Note that $R_1(U, P)$ is defined elementwise and that with piecewise linears in space, the Laplacian ΔU is zero. In the computations presented below, we chose $\kappa_3 = 0$

corresponding to shutting off the artificial viscosity. Note that $R_1(U,P)+R_2(U,P)$ bounds the residual of the momentum equation, with the Laplacian term bounded by the second order difference quotient $D_2(U)$ arising from the jumps of normal derivatives across element boundaries.

The order of the G^2-method with polynomials of degree p in space/time is generally $p+1/2$, see [3]. For more details on the G^2-method see [11].

2.5. **The G^2-method for turbulent flow.** In [13] we present the G^2-method for the averaged Navier-Stokes equations (2.4) using the subgrid model (2.6), with $\check{\nu}_{ij}=\nu_T$: Find $(U_h,P_h)\in V^\beta\times Q^\beta$, such that for $n=1,2,...,N$,

$$
\begin{aligned}
&(\dot{U}_h+(U_h\cdot\nabla)U_h,v)_n-(P_h,\operatorname{div}v)_n+(q,\operatorname{div}U_h)_n\\
&+(\tilde{\nu}\epsilon(U_h),\epsilon(v))_n+(\delta_1 a(U_h;U_h,P_h),a(U_h;v,q))_n\\
&-(\check{\tau}^h(U_h),\nabla v)_n+(\delta_2\operatorname{div}U_h,\operatorname{div}v)_n+([U_h^{n-1}],v_+^{n-1})\\
&=(f,v+\delta_1 a(U_h;v,q))_n\quad\forall(v,q)\in V_n^\beta\times Q_n^\beta,
\end{aligned}
\tag{2.14}
$$

where $a(w;v,q)=D_{w,t}v+\nabla q-\nu\Delta v$ with the Laplacian defined elementwise, $\delta_1=\frac{1}{2}(k_n^{-2}+|U_h|^2h_n^{-2})^{-1/2}$ in the convection-dominated case $\tilde{\nu}<U_hh_n$ and $\delta_1=\kappa_1h^2$ otherwise, $\delta_2=\kappa_2h$ if $\tilde{\nu}<U_hh_n$ and $\delta_2=\kappa_2h^2$ otherwise, with κ_1 and κ_2 positive constants of unit size, $\tilde{\nu}=\max(\nu+\nu_T,\kappa_3|R(U_h,P_h)|h^2)$, where ν_T is the turbulent eddy viscosity from (2.6), and $\check{\tau}^h$ is the algebraic part from (2.6), and $R(U_h,P_h)=\sum_{i=1}^4R_i(U_h,P_h)$ with

$$
\begin{aligned}
R_1(U_h,P_h) &= |\dot{U}_h+U_h\cdot\nabla U_h+\nabla P_h-f+\operatorname{div}\check{\tau}^h(U_h)-\tilde{\nu}\Delta U_h|,\\
R_2(U_h,P_h) &= \tilde{\nu}D_2(U_h),\\
R_3(U_h,P_h) &= |[U_h^{n-1}]|/k_n\quad\text{on } S_n,\\
R_4(U_h,P_h) &= |\operatorname{div}U_h|,
\end{aligned}
$$

with $D_2(U_h)$ defined by (2.13), and where $R_1(U_h,P_h)$ is defined elementwise and with piecewise linears in space, the Laplacian ΔU_h is zero. In the computations presented below, we chose $\kappa_3=0$ corresponding to shutting off the artificial viscosity.

2.6. **The cG(1)cG(1)-method for turbulent flow.** The cG(1)cG(1)-method is a variant of the above G^2-method using the continuous Galerkin method cG(1) in time instead of a discontinuous Galerkin method. With cG(1) in time the trial functions are continuous piecewise linear and the test functions piecewise constant. The cG(1)cG(1)-method for the averaged Navier-Stokes equations (2.4), using the subgrid model (2.6) with $\check{\nu}_{ij}=\nu_T$ reads: For $n=1,...,N$, find $(U_h^n,P_h^n)\in V_n^0\times Q_n^0$, with $V_n^0=W_{0n}^3$ and $Q_n^0=W_n$, such that

$$
\begin{aligned}
&(\frac{U_h^n-U_h^{n-1}}{k_n},v)+(\hat{U}_h^n\cdot\nabla\hat{U}_h^n+\nabla P_h^n,v+\delta_1(\hat{U}_h^n\cdot\nabla v+\nabla q))\\
&+\delta_2(\operatorname{div}\hat{U}_h^n,\operatorname{div}v)+(\nabla\cdot\hat{U}_h^n,q)+(\tilde{\nu}\nabla\hat{U}_h^n,\nabla v)-(\check{\tau}_n^h(\hat{U}_h^n),\nabla v)\\
&=(f^n,v+\delta_1(\hat{U}_h^n\cdot\nabla v+\nabla q))\quad\forall(v,q)\in V_n^0\times Q_n^0,
\end{aligned}
\tag{2.15}
$$

where $\hat{U}_h^n=\frac{1}{2}(U_h^n+U_h^{n-1})$. This method corresponds to a second order accurate Crank-Nicolson time-stepping, but the stabilization suffers from an inconsistency up to the term

$\delta_1 \dot{u}$ resulting from using piecewise constant test functions. The inconsistency seems to be be acceptable unless $\dot{u}$ is large, and we use cG(1)cG(1) in the computations presented below.

3. A posteriori error estimation for turbulent flow

To derive a posteriori error estimates for the averaged Navier-Stokes equations (2.4), we have to take into account both the numerical error from discretization and the modeling error from unresolved subgrid scales. Aiming at error control of the quantity $\int_Q (u^h - U_h) \cdot \psi \; dx \; dt$ in $Q = \Omega \times I$, with $\psi \in L_2(I; [L_2(\Omega)]^3)$ given, we introduce the following linearized dual problem: Find $(\varphi, \theta) \in L_2(I; [H_0^1(\Omega)]^3 \times L_2(\Omega)) \equiv W$ such that

$$
\begin{aligned}
-\dot{\varphi} - (u^h \cdot \nabla)\varphi + \nabla U_h \cdot \varphi + \nabla\theta - \tilde{\nu}\Delta\varphi &= \psi \qquad \text{in } Q \\
\operatorname{div} \varphi &= 0 \qquad \text{in } Q \\
\varphi &= 0 \qquad \text{on } \Gamma \times I, \\
\varphi(\cdot, T) &= 0 \qquad \text{in } \Omega,
\end{aligned}
\tag{3.1}
$$

where $(\nabla U_h \cdot \varphi)_j = (U_h)_{,j} \cdot \varphi$, and we note that we use the viscosity $\tilde{\nu}$, including the eddy viscosity ν_T. Depending of the choice of ψ, the quantity $\int_Q (u^h - U_h) \cdot \psi \; dx \; dt$ may represent different norms of the error or, by the Riesz representation theorem, any linear functional of the error, such as the mean drag force, for example.

Theorem 1. *With u^h the solution to (2.4) and $\psi \in L_2(I; [L_2(\Omega)]^3)$ given, we have the following error representation formula for $(U_h, P_h) \in V^\beta \times Q^\beta$:*

$$
\begin{aligned}
\int_Q (u^h - U_h) \cdot \psi \; dx \; dt = &\int_Q R_1(U_h, P_h) \cdot \varphi \; dx \; dt + \int_Q R_4(U_h, P_h) \cdot \theta \; dx \; dt \\
&+ \frac{1}{2} \sum_{n=1}^{N} \sum_{K \in \mathcal{T}_n} \int_{\partial K \times I_n} R_2(U_h, P_h) \cdot \varphi \; ds \; dt \\
&+ \sum_{n=1}^{N} \int_\Omega R_3(U_h, P_h) \cdot \varphi(t_{n-1}) \; dx \\
&+ \int_Q R_M(u, U_h) \cdot \varphi \; dx \; dt
\end{aligned}
$$

where (φ, θ) are the solutions to the dual problem (3.1), and

$$
\begin{aligned}
R_1(U_h, P_h) &= f - (\dot{U}_h + U_h \cdot \nabla U_h + \nabla P_h - \tilde{\nu}\Delta U_h + \operatorname{div} \check{\tau}^h(U_h)), \\
R_2(U_h, P_h) &= \tilde{\nu} \left[\frac{\partial U_h}{\partial n} \right] \\
R_3(U_h, P_h) &= [U_h^{n-1}] \;\; \text{on } S_n, \\
R_4(U_h, P_h) &= \operatorname{div} U_h, \\
R_M(u, U_h) &= \operatorname{div} \check{\tau}^h(U_h) - (\operatorname{div} \tau^h(h) + \nu_T \Delta u^h),
\end{aligned}
$$

with $(\check{\tau}^h, \nu_T)$ from (2.14).

We note that Theorem 1 is valid for any $(U_h, P_h) \in V^\beta \times Q^\beta$. If (U_h, P_h) are computed using a Galerkin method, for example the cG(1)cG(1)-method with $\delta_1 = \delta_2 = 0$, then we may use the Galerkin orthogonality property for the discretization error to subtract interpolants of the dual solution (φ, θ), and then estimate the interpolation errors in terms of derivatives of (φ, θ) and powers of the space and time discretization parameters. As an example, we present the corresponding error estimates for the cG(1)cG(1)-method, and for simplicity we consider the case when $\delta_1 = \delta_2 = 0$.

Theorem 2. *If u^h solves (2.4), $(U_h, P_h) \in V_n^0 \times Q_n^0$ solves (2.15) with $\delta_1 = \delta_2 = 0$, and $\psi \in L_2(I; [L_2(\Omega)]^3)$ is given, then*

$$
\begin{aligned}
|\int_Q (u^h - U_h)\cdot\psi \; dx \; dt| \leq \sum_{n=1}^N \int_{I_n} \sum_{K\in\mathcal{T}_n} \{ \int_K \{ \; & |R_M(u,U_h)|\cdot|\varphi| \\
& + |R_1(U_h)|\cdot(C_h h_{n,K}^m \|D^m\varphi\|_{\infty,K,n} + C_k k_n \|\dot\varphi\|_{\infty,K,n}) \\
& + |R_4(U_h)| \; (C_h h_{n,K}^m \|D^m\theta\|_{\infty,K,n} + C_k k_n \|\dot\theta\|_{\infty,K,n}) \; \} \; dx \\
& + \int_{\partial K} |R_2(U_h)|\cdot(C_h h_{n,K}^m \|D^m\varphi\|_{\infty,\partial K,n} + C_k k_n \|\dot\varphi\|_{\infty,\partial K,n}) \; ds \; \} \; dt,
\end{aligned}
$$

for $m = 1, 2$, where $\|\cdot\|_{\infty,K,n} \equiv \max_{(x,t)\in K\times I_n} |\cdot|$, $|w| \equiv (|w_1|, ..., |w_n|)$ for $w \in \mathbb{R}^n$, $h_{n,K} = \max_{t\in I_n} h_K(t)$ with $h_K(t)$ the diameter of element K at t, D^m measures derivatives with respect to x of order m, and C_h, C_k represents interpolation constants.

Remark 3. *We note that there are several possibilities to pose the dual problem. In (3.1) we chose to include the turbulent viscosity ν_T in the dual problem, but we could alternatively have chosen to only use the viscosity ν, which would have given a different modeling residual $R_M(u, U_h)$. The motivation for using the larger turbulent viscosity is improved regularity of the dual solution (φ, θ).*

Remark 4. *If $\delta_1, \delta_2 \neq 0$, we may view the stabilizing terms as a modification of the continuous equation, which we solve by a standard Galerkin method, according to Section **??**. We then modify the dual problem accordingly, to obtain Galerkin orthogonality for the discretization error of the solution of the stabilized equations.*

4. Numerical results

In this section we investigate different aspects of error analysis for turbulent flow, using the ideas developed in the previous sections. In [12] a computational study of transition to turbulence in shear flow is conducted which we use here as an example of a turbulent flow, and we make some comparisons with laminar flows from [11]. In the computations we use the cG(1)cG(1)-method from Section 2.6, on the unit cube with a regular tetrahedral mesh with $65 \times 65 \times 65$ nodes. We use periodic boundary conditions in the streamwise x_1-direction and in the spanwise x_3-direction, and we have streamwise velocity ± 1 on top and bottom. In Fig.1 we see the velocity isosurfaces for $|u| = 0.2$, after transition to turbulence in a Couette flow described in [12], where we have used $\nu = 1/10000$.

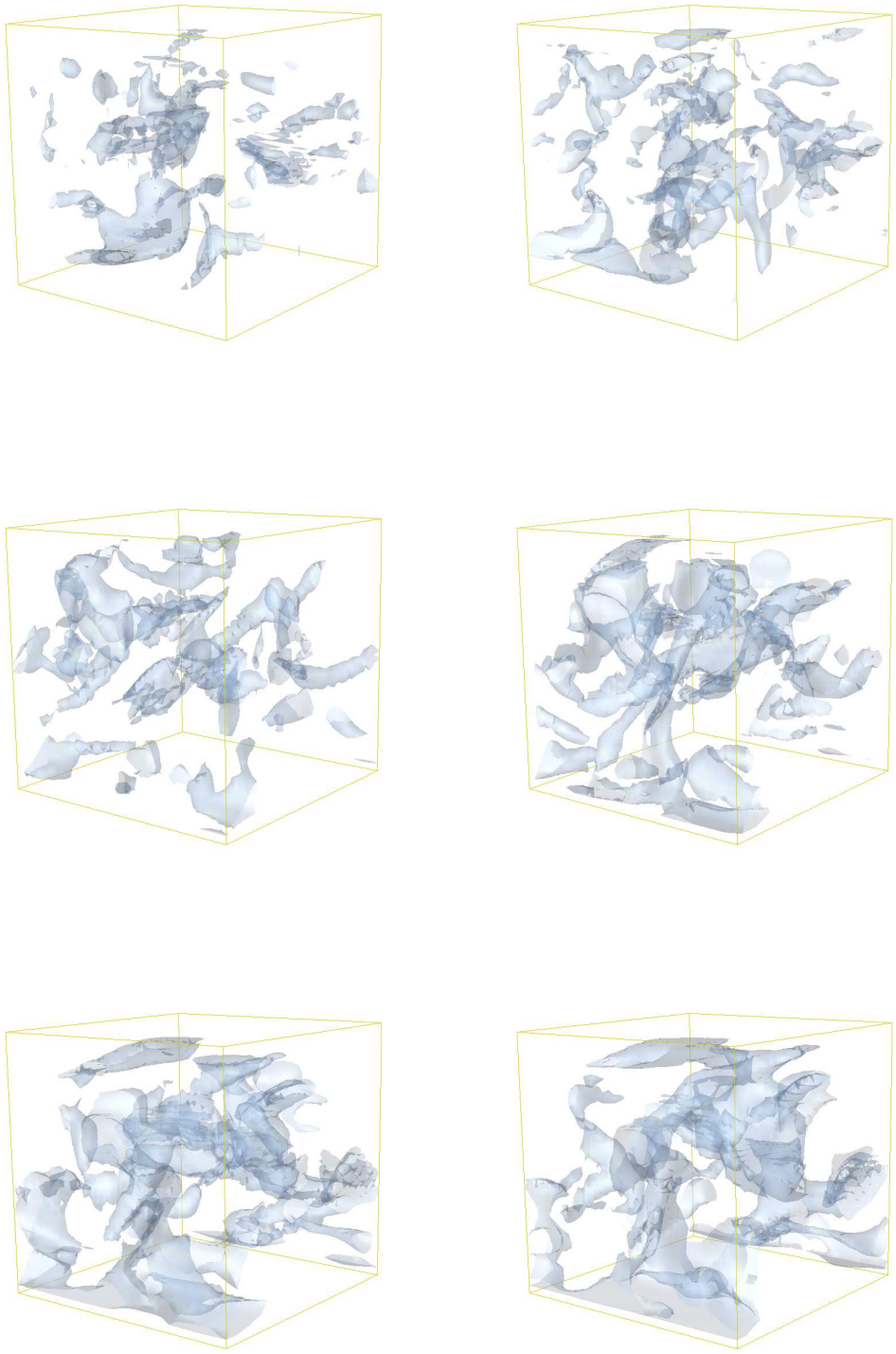

FIGURE 1. Velocity isosurfaces for $|u| = 0.2$ in Couette flow for $t = 20, 22, 24, 26, 28, 30$

4.1. **Estimation of the modeling residual.** From Section 3 we know that the total computational error, when we compute approximate solutions to (2.4), is a sum of a discretization error and a modeling error. We may compute either with or without a subgrid model. If we do not use a subgrid model in the computations, we still need to estimate the modeling error. We may then use a subgrid model to estimate the modeling error, without using the subgrid model in the computations. For example, we may use the scale similarity model (2.8), or we may use the ideas in [7, 8, 9, 10] to extrapolate $\tau_{ij}^h(u)$ from coarser scales $2h$ and $4h$. The extrapolation formula then takes the form

$$\tilde{\tau}_{ij}^h(U_h) = g(\tau_{ij}^h(U_h), \tau_{ij}^{2h}(U_h), \tau_{ij}^{4h}(U_h)) \tag{4.1}$$

with $g(a,b,c)$ from [11] defined by

$$g(a,b,c) = (1 - (\frac{c - b^{4h}}{b^{4h} - a^{4h}})^{-n}) \frac{b^{4h} - a^{4h}}{\frac{c - b^{4h}}{b^{4h} - a^{4h}} - 1} \tag{4.2}$$

and $2^{-n}h$ is the finest scale present in the exact solution. (4.2) is based on an Ansatz of the form

$$E_h(v,w)(x) = C(x)h^{\mu(x)} \tag{4.3}$$

for covariances of the form $E_h(v,w) = (vw)^h - v^h w^h$, and a fundamental question is now if the Ansatz (4.3) is valid for $\tau_{ij}^h(u)$ in the computations, that is if we have scale similarity. We test this hypothesis for the computed solution U_h, where we compute $a_{ij}^1 = \tau_{ij}^{2h}(U_h) - \tau_{ij}^h(U_h)$, $a_{ij}^2 = \tau_{ij}^{4h}(U_h) - \tau_{ij}^{2h}(U_h)$, and $a_{ij}^3 = \tau_{ij}^{8h}(U_h) - \tau_{ij}^{4h}(U_h)$. As an approximation of the running average operator on the scale h we use a projection $[\cdot]^h$ onto the space of piecewise constant functions on the mesh corresponding to h. The spaces of piecewise constant functions on successively uniformly refined meshes form a Haar MRA of the space $L_2(\Omega)$, where the uniform refinement, dividing one tetrahedron into eight new ones, is described in Fig.2.

In [7, 8] covariances with respect to Haar MRA is investigated, and it is shown that $[u_i u_j]^h - [u_i]^h [u_j]^h = \sum_{k \le h} \{\text{Haar coeff. of } u_i \times \text{Haar coeff. of } u_j, \text{ on scale } k\}$, and $a_{ji}^1, a_{ji}^2, a_{ji}^3$ now represents the sum of Haar coefficients of $\tau^{8h}(U_h)$ on the scales $2h$, $4h$, and $8h$ respectively. If Ansatz (4.3) is valid, $\tau^{8h}(U_h)$ is scale similar and thus possible to extrapolate, a_{ji}^1, a_{ji}^2, and a_{ji}^3 should decrease regularly. If we have scale similarity in the coarser scales $2h$, $4h$, and $8h$, we anticipate scale similarity in finer scales, since we assume that we are in the inertial range. In Fig.3 we present the L_1-norms of a_{ji}^1, a_{ji}^2, and a_{ji}^3, showing that we have a certain degree of scale similarity, and we find that the decrease is typically by a factor 1.5. From [7, 8] we have a dependence $a_{ij}^k \sim (2^k h)^{\delta_i + \delta_j}$, for δ_i, δ_j being the Hölder exponents of u_i and u_j respectively. If we assume that $\delta_i = \delta_j = \delta$, we get that $a_{ij}^{k+1}/a_{ij}^k = (2^{k+1}h)^{2\delta}/(2^k h)^{2\delta} = 2^{2\delta} = 1.5$, which gives that $\delta = \log(1.5)/2\log(2) \approx 0.29$, which is very close $\delta = 1/3$, corresponding to the velocity being Hölder continuous with exponent $1/3$, which is consistent with the *Kolmogorov 5/3-law* for the energy spectrum, see [4]. The results in Fig.3 support the Ansatz (4.3), although we note that these are global results (using the global L_1-norm).

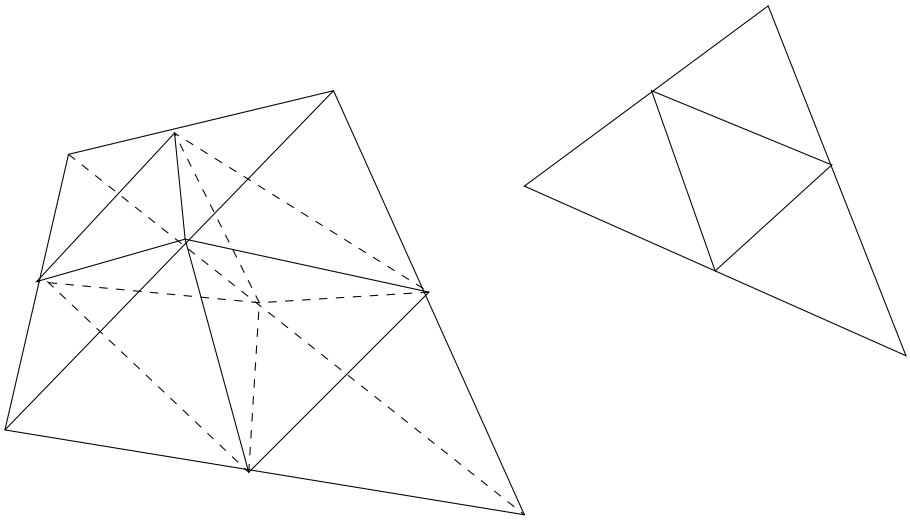

FIGURE 2. Haar MRA generated from successively refining unstructured tetrahedral and triangular meshes, in 3d and 2d respectively.

If we use a subgrid model in the computations we need to estimate the difference $F_h(u) - \hat{F}_h(U_h)$, and we are thus lead to model terms of the form $\Delta_h = \tau_{ij}^h(u) - \hat{\tau}_{ij}^h(U_h)$. We may base our estimation of Δ_h on extrapolation, and we then have to find approximations to $\Delta_{2h} = \tau_{ij}^{2h}(u) - \hat{\tau}_{ij}^{2h}(U_{2h})$ and $\Delta_{4h} = \tau_{ij}^{4h}(u) - \hat{\tau}_{ij}^{4h}(U_{4h})$. Using the Ansatz 4.3, may use the approximation $\tau_{ij}^{2h}(u) \approx \tilde{\tau}_{ij}^{2h}(U_h)$, where $\tilde{\tau}_{ij}^{2h}(U_h) = \tilde{g}_{2h}(\tau_{ij}^h(U_h), \tau_{ij}^{2h}(U_h), \tau_{ij}^{4h}(U_h))$ with $\tilde{g}_{2h}(a,b,c)$ defined by

$$\tilde{g}_{2h}(a,b,c) = (1 - (\frac{c-b^{4h}}{b^{4h}-a^{4h}})^{1-n}) \frac{c-b^{4h}}{\frac{c-b^{4h}}{b^{4h}-a^{4h}} - 1} \tag{4.4}$$

and in a similar way we get $\tau_{ij}^{4h}(u) \approx \tilde{\tau}_{ij}^{4h}(U_h)$, where $\tilde{\tau}_{ij}^{4h}(U_h) = \tilde{g}_{4h}(\tau_{ij}^h(U_h), \tau_{ij}^{2h}(U_h), \tau_{ij}^{4h}(U_h))$ with $\tilde{g}_{4h}(a,b,c)$ defined by

$$\tilde{g}_{4h}(a,b,c) = (1 - (\frac{c-b^{4h}}{b^{4h}-a^{4h}})^{2-n}) \frac{c-b^{4h}}{1 - \frac{b^{4h}-a^{4h}}{c-b^{4h}}}. \tag{4.5}$$

We then get $\Delta_h \approx \tilde{\Delta}_h = g(0, \tilde{\Delta}_{2h}, \tilde{\Delta}_{4h})$, with $\tilde{\Delta}_{2h} = \tilde{\tau}_{ij}^{2h}(U_h) - \hat{\tau}_{ij}^{2h}(U_{2h})$, $\tilde{\Delta}_{4h} = \tilde{\tau}_{ij}^{4h}(U_h) - \hat{\tau}_{ij}^{4h}(U_{4h})$, and $g(a,b,c)$ defined by (4.2).

4.2. **Discretization error vs. modeling error.** We now use the results in Section 3 to estimate the error in the computation of the turbulent flow described above, where we use the velocity from $t = 20$ as initial condition. We consider the initial condition to be exact, and we compute to $t = 30$. From Theorem 2, we have that

$$|\int_Q (u^h - U_h) \cdot \psi \; dx \; dt| \leq e_D + e_M,$$

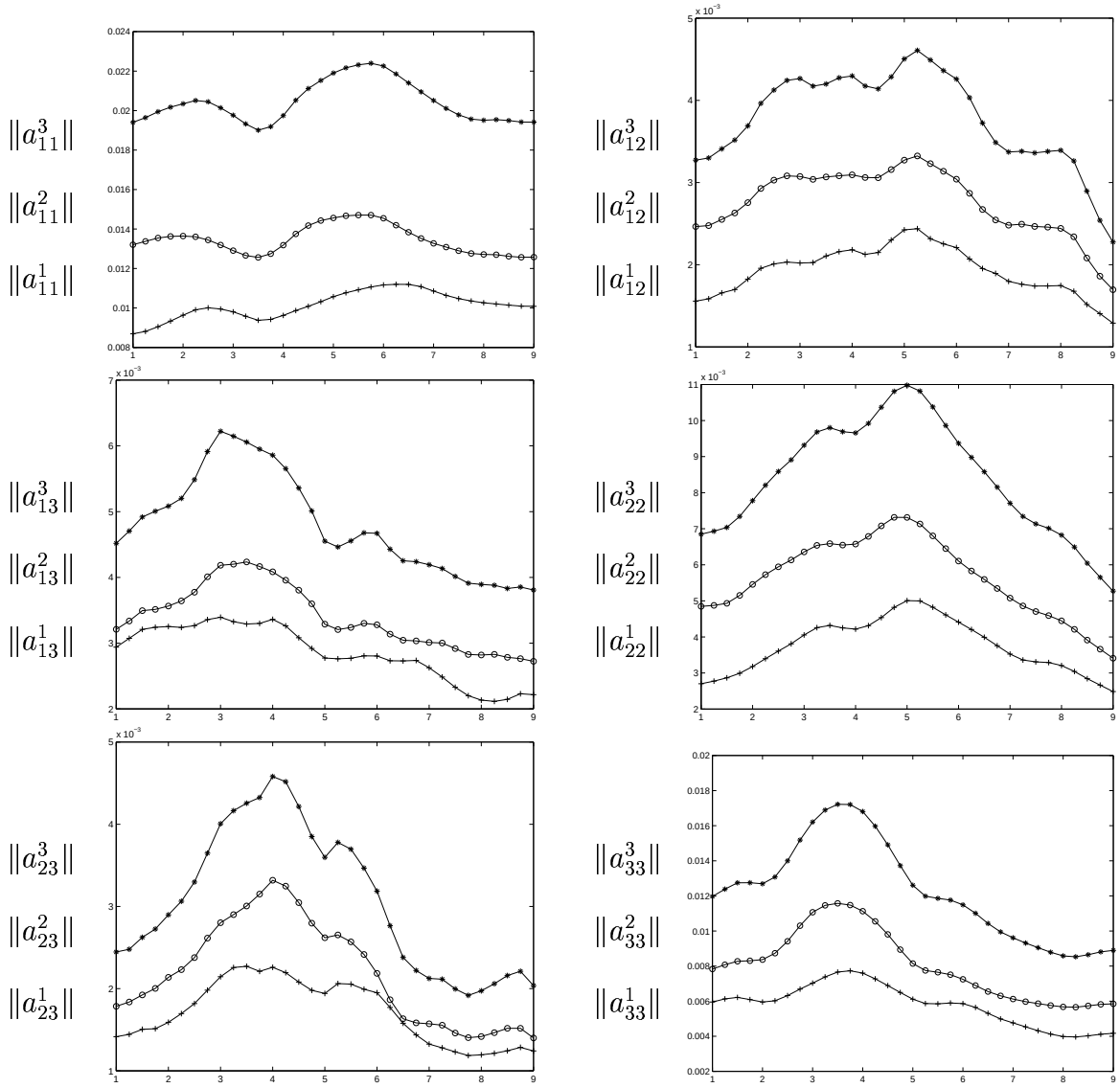

FIGURE 3. $\|a_{ij}^1\|_1$ ('+'), $\|a_{ij}^2\|_1$ ('o') and $\|a_{ij}^3\|_1$ ('*')

where

$$e_D = \sum_n \int_{I_n} \sum_{K \in \mathcal{T}_n} \{ \int_K \{ \, |R_1(U_h)| \cdot (C_h h_{n,K}^m \|D^m \varphi\|_{\infty,K,n} + C_k k_n \|\dot{\varphi}\|_{\infty,K,n})$$
$$+ |R_4(U_h)| \, (C_h h_{n,K}^m \|D^m \theta\|_{\infty,K,n} + C_k k_n \|\dot{\theta}\|_{\infty,K,n}) \, \} \, dx$$
$$+ \int_{\partial K} |R_2(U_h)| \cdot (C_h h_{n,K}^m \|D^m \varphi\|_{\infty,\partial K,n} + C_k k_n \|\dot{\varphi}\|_{\infty,\partial K,n}) \, ds \, \} \, dt,$$

represents a discretization error and

$$e_M = \sum_n \int_{I_n} \sum_{K \in \mathcal{T}_n} \int_K |R_M(u, U_h)| \cdot |\varphi| \; dx \; dt,$$

represents a modeling error. Here $h = 1/64$ in the definition of u^h, which corresponds to the uniform mesh size, and $\nu = 1/10000$, so that the underlying flow contains finer scales than h. The effective Reynolds number in the computations is further discussed in Section 4.5. We use no subgrid model, and we are now going to estimate e_D and e_M using Theorem 2. For both the discretization and the modeling error we need to approximate the dual solutions (φ, θ). The discretization residuals are directly computable from the approximate solutions (U_h, P_h), whereas the modeling residual $R_M(u, U_h)$ has to be estimated. If the modeling error without a subgrid model is neglible compared to the discretization error, then we do not need a subgrid model. If on the other hand the modeling error dominates, we need to either use a subgrid model or to refine the computational mesh. Here we use (2.8), with $C_L = 1$, to estimate the modeling residual without a subgrid model. In the estimate of the discretization residual we use $C_h = 1/8$ and $C_k = 1/2$, which are approximations of the interpolation constants motivated by a simple analysis on a reference element.

In Fig.4 we present estimates of the relative discretization error and modeling error, normalized by $U_T = \|U_h(30)\|_1 \approx 0.43$ ($\|\cdot\|_1 = \int_\Omega |\cdot| \; dx$), in the computation of a space-time average over $\omega \times [30 - d(\omega), 30]$ of the solution u^h, with ω being a spatial cube with side length $d(\omega)$, centered at $(0.5, 0.5, 0.5)$. This corresponds to $\psi = \chi_{\omega \times [30-d(\omega),30]} / |\chi_{\omega \times [30-d(\omega),30]}|$ in the dual problem (3.1), where χ_D is the characteristic function for D, and $|D|$ denotes the space-time volume of D. Fig.4 should be understood as the errors for different starting times, assuming that the particular starting solutions at these starting times are exact.

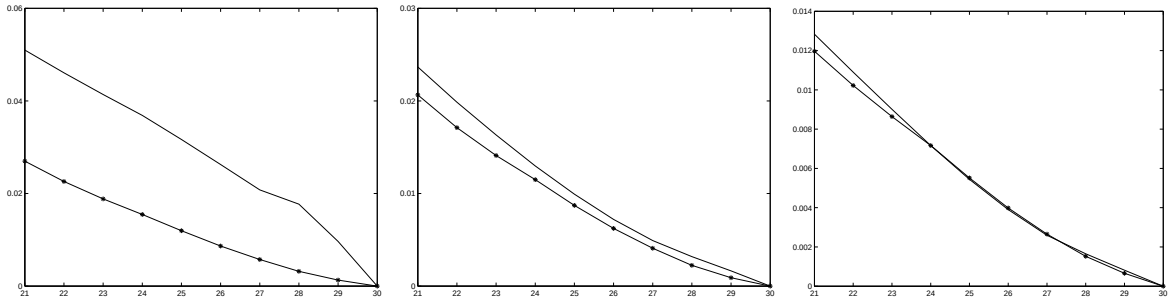

FIGURE 4. e_D/U_T ('-') and e_M/U_T ('*') for $d(\omega) = 0.125$ (left), 0.25 (middle), 0.5 (right)

We find that the discretization error and the modeling error are of the same order in this computation, both errors are less than a few percent of the size of the solution, and the errors of course increase if we compute over a longer time. In the estimate of the discretization error we have neglected the residual $R_2(U_h)$, since the other residuals

dominate for ν small when we do not use an eddy viscosity subgrid model. We note that both e_D and e_M are larger for smaller space-time averages, supporting our belief that it is harder to compute smaller space-time averages than larger. We also note that the difference between e_D and e_M is smaller for larger $d(\omega)$.

In Fig 5 we present plots of the discretization residuals $R_1(U_h, P_h)$, $R_4(U_h)$ and the modeling residual $R_M(u, U_h)$. We see that first $R_1(U_h, P_h)$ is large in the middle of the domain, but after a while $R_1(U_h, P_h)$ is largest at the top and bottom. This is because the flow is changing from a Couette profile (linear profile in the vertical direction of the streamwise velocity), where the residual is large in the middle, into a solution with small velocities in the middle and sharp boundary layers at top and bottom that the mesh is not capable of resolving, causing large residuals in these layers. The modeling residual $R_M(u, U_h)$ behaves similarily, whereas $R_4(U_h)$, on the other hand, is more isotropic.

Remark 5. *In the computation of the dual problem we use a $cG(1)cG(1)$-method, corresponding to the method used for the primal problem, on a uniform tetrahedral mesh with $32 \times 32 \times 32$ nodes, and we approximate both u^h and U_h with U_h, projected onto this mesh.*

Remark 6. *Since we use a stabilized Galerkin method there are also terms from the stabilization present in e_D and e_M. In this study we assume these terms to be small compared to the other terms since they are weghted by a small stabilization parameter.*

4.3. **Error propagation and the dual problem.** Theorem 1 shows that the error is of the form of space-time integrals of residuals times the solutions to a dual problems. The residuals measure how well the computed solution satisfies the differential equation, and the solution of the dual problem determines how the residual influences the particular error measure considered. We may alternatively view the dual problem as describing how the error, produced through a non zero residual, is propagated in space-time. The linearized dual Navier-Stokes equations are closely related to the linearized Navier-Stokes equations [12], where the linearized dual Navier-Stokes equations describe the propagation of errors and the linearized Navier-Stokes equations describe the propagation of perturbations.

The sizes of the residuals are fairly constant in time, whereas the solution of the dual problem, on the other hand, is growing (backwards) in time. We consider the example of computing the space-time average from Section 4.2. In Fig.7 we show the dual solutions for $d(\omega) = 0.5, 0.25, 0.125$, and in Fig.6 we plot the L_1-norms of the dual solutions. In the initial phase (for backward time) the dual solutions grow through the action of the force ψ during the time interval $[30 - d(\omega), 30]$. This initial growth is larger for small $d(\omega)$, which may be explained by the larger quotient $q(d(\omega)) = \text{surface area/volume} = 6d(\omega)^2/d(\omega)^3 = 6/d(\omega)$ for smaller $d(\omega)$. This is because the divergence free condition, which is active in increasing the dual solution, depends on $q(d(\omega))$. Since this phenomena is connected to the divergence free condition, we can observe the same phenomena also in the simple problem

$$\dot{\varphi} + \nabla q = \psi, \quad \nabla \cdot \varphi = 0, \tag{4.6}$$

shown in Fig.6.

In the next phase, after the force ψ is shut off, there is a growth due to the reaction term in (3.1). This growth is later neutralized by cancelations, causing diffusion to dominate,

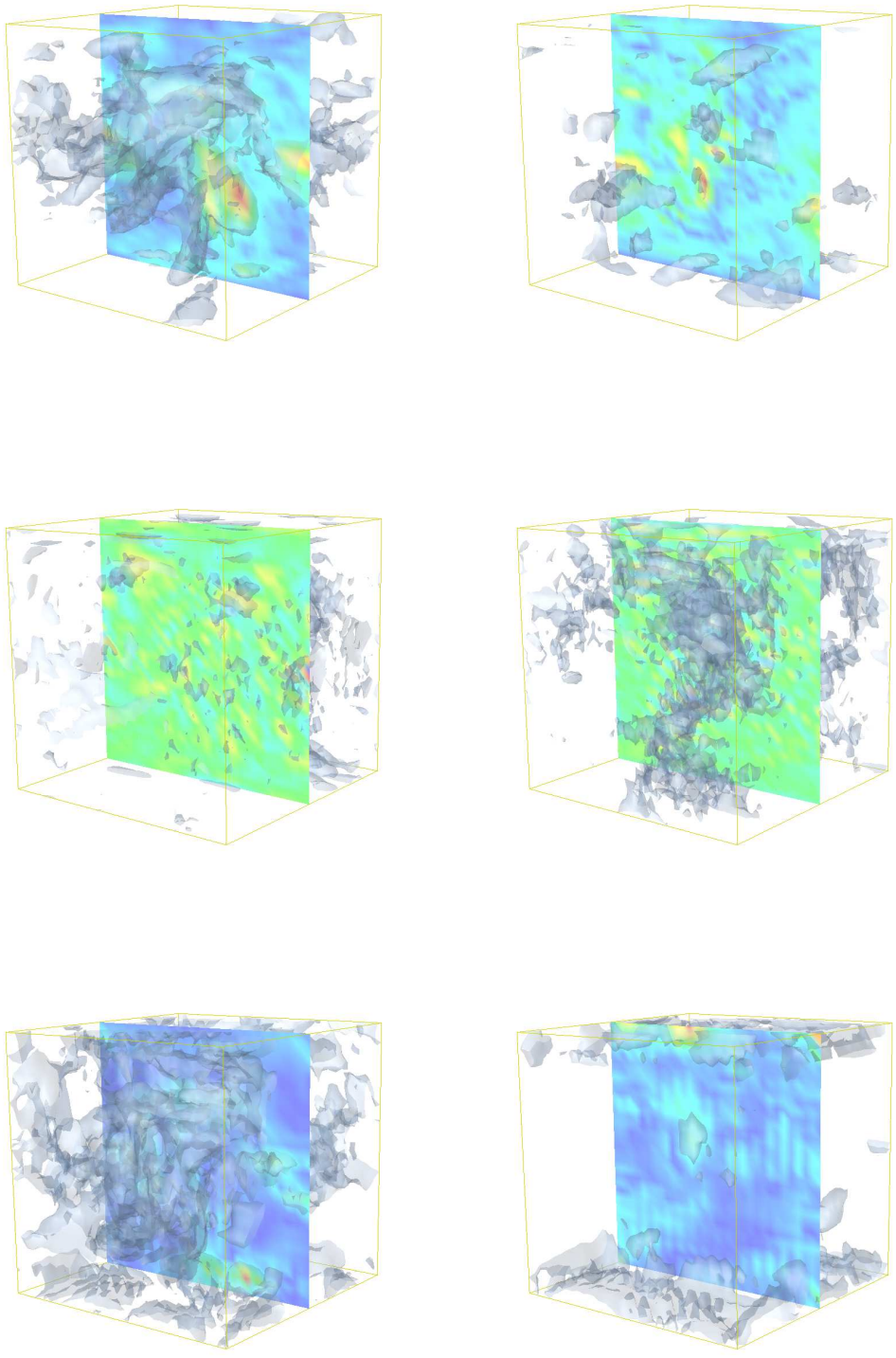

FIGURE 5. High value isosurf.: $|R_1(U_h, P_h)|$ (upper), $|R_4(U_h)|$ (middle), $|R_M(u, U_h)|$ (lower), $t = 20, 30$

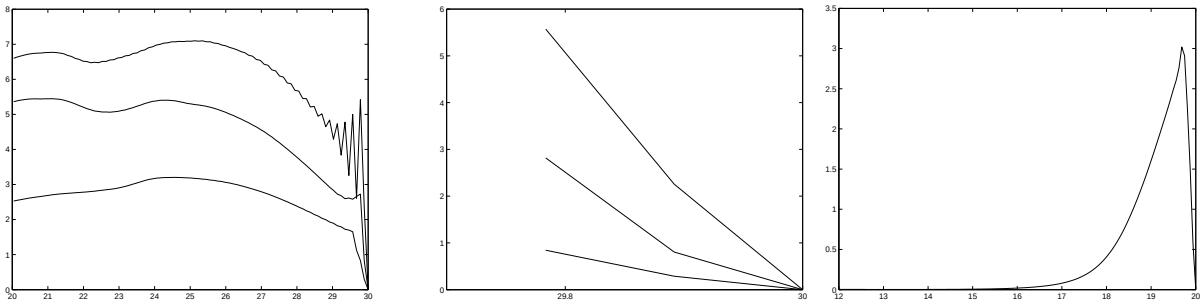

FIGURE 6. $\|\varphi\|_1$ for $d(\omega) = 0.5, 0.25, 0.125$ (left), $\|\varphi\|_1$ for problem (4.6) $d(\omega) = 0.5, 0.25, 0.125$ (middle), laminar bluff body: $\|\varphi(t)\|_1$ for $d(\omega) = 0.25$ (right).

and the dual solution slowly decays. Cancelations cause the growth to be weaker for larger $d(\omega)$. The intensity of the growth through the reaction term is connected to the irregularity of the computed solution, through the term $\nabla U_h \cdot \varphi$, and cannot be observed for laminar flows, where the diffusion dominates this reaction term. As an example, in Fig.6 we plot the dual solution for $d(\omega) = 0.25$ in the case of a laminar bluff body flow from [11], where ω is centered at $(2.5, 0.5, 0.5)$. We note that there is no growth of the dual problem due to the reaction term, instead the solution decays monotonically when the force ψ is shut off.

4.4. **Evaluation of different subgrid models.** In Section 4.2 we estimated the discretization error and the modeling error, when we did not use a subgrid model. We now consider the problem of estimating the modeling error for different subgrid models. We seek u^h, with $h = 1/32$, and we use $\tau^h(U_{h/2})$ as an approximation of the true Reynolds stresses $\tau^h(u)$. We compare the scale similarity model (2.8) and the Smagorinsky model (2.9).

Experience tells us, see e.g. [5], that neither an eddy viscosity model nor a scale similarity model is perfect as a stand alone subgrid model. Instead a combination of the two seems potentially better. A possible explanation is that $\tau^h(u)$ is combined of a low frequency part and a high frequency part, and that an eddy viscosity model has typically a better chance to model the high frequency part whereas a scale similarity model typically has a better chance to model the low frequency part. As a test we try to fit the the scale similarity model (2.8) and the eddy viscosity model (2.9) to our approximation of the true Reynolds stresses $\tau^h(u) \approx \tau^h(U_{h/2})$, by changing the constants C_S and C_L, where we base the models on the solution $U_{h/2}$, projected onto the scale h.

We find that we are unable to fit the Smagorinsky model by changing C_S. Using the scale similarity model we are able to reduce the modeling error by 20%, for $C_L = 0.25$.

Remark 7. *We note that this test does not rule out the Smagorinsky model as a possible subgrid model, since it is known* [5] *that eddy viscosity models does poor in these type of tests, possibly because of the form of the Reynolds stresses being composed of a low frequency part as well as a high frequency part. We may split the Reynolds stresses as*

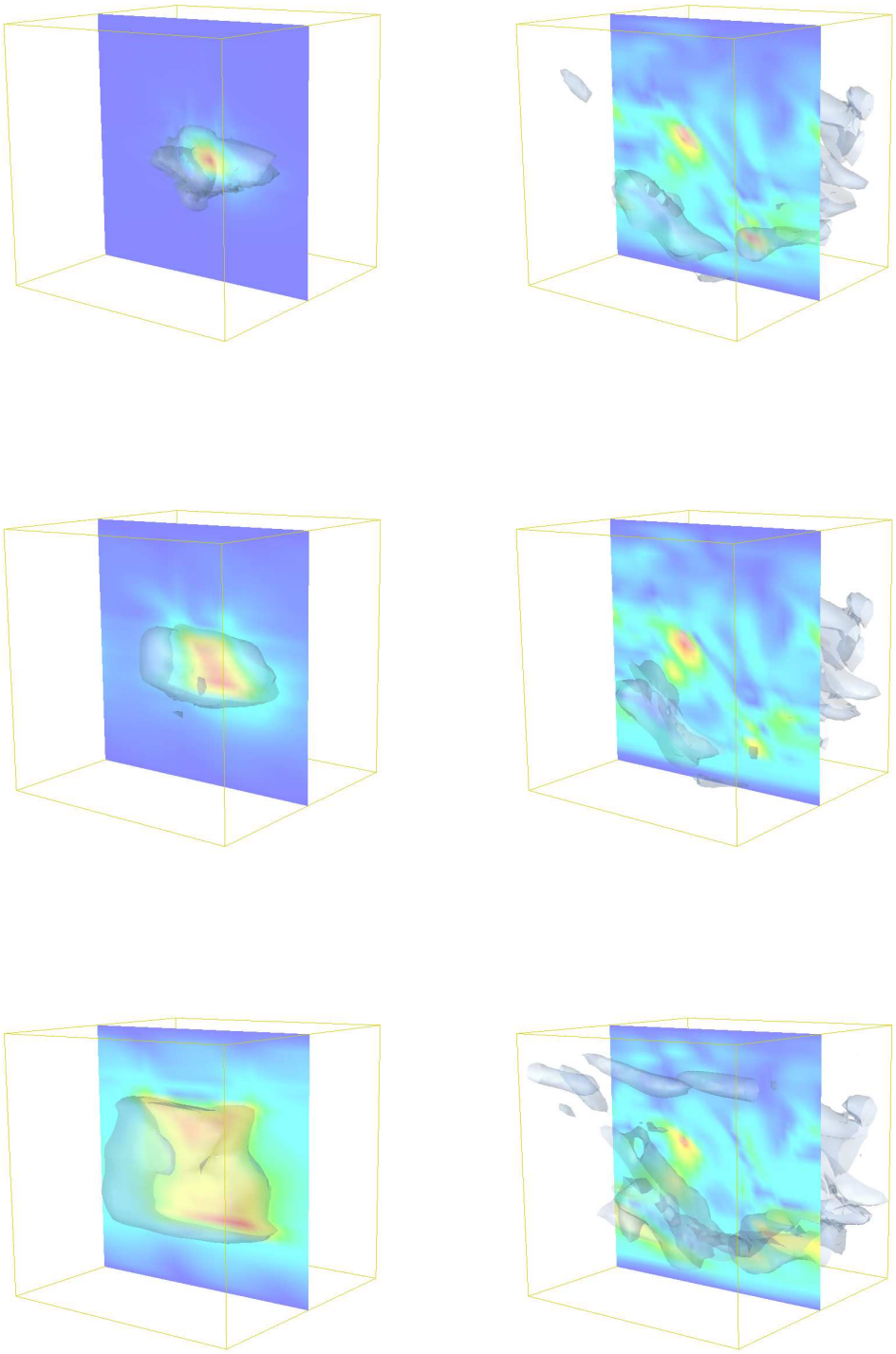

FIGURE 7. Streamwise high dual velocity isosurfaces: $d(\omega) = 0.125$ (upper), $d(\omega) = 0.25$ (middle), $d(\omega) = 0.5$ (lower), for $t = 29.5, 24$

$\tau^h(u) = (\tau^h(u))^H + (\tau^h(u) - (\tau^h(u))^H)$, $H > h$, *where a scale similarity model might be a good model for the low frequency part* $(\tau^h(u))^H$, *and an eddy viscosity model would be a good model for the high frequency part* $\tau^h(u) - (\tau^h(u))^H$.

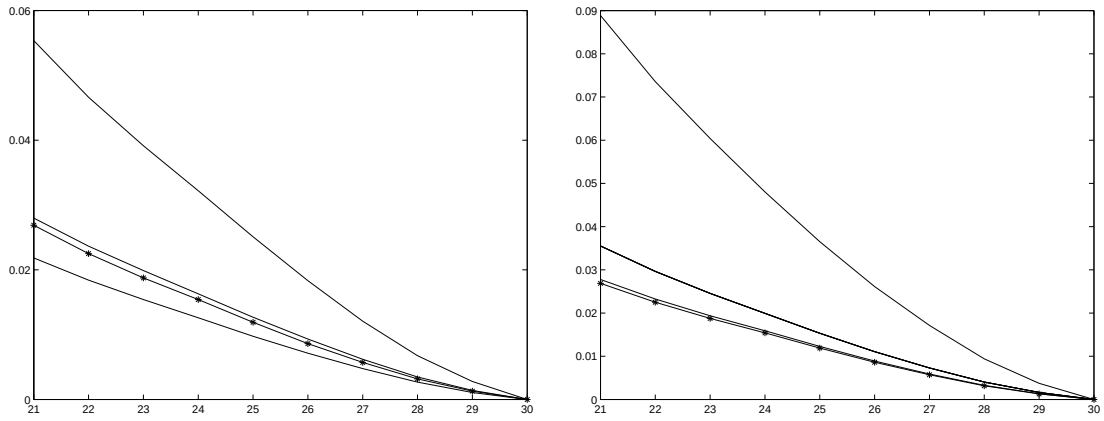

FIGURE 8. e_M/U_T for $C_L = 0.25, 0.5, 1.0$ ('-') and $C_L = 0$ ('*') (left), and $C_S = 0.05, 0.1, 0.2$ ('-') and $C_S = 0$ ('*') (right), for $d(\omega) = 0.125$

4.5. **What is the effective Reynolds number?** The use of a stabilized Galerkin method corresponds to solving a perturbed equation using a standard Galerkin method, see [13]. A part of the stabilizing terms typically corresponds to an increased effective viscosity in the computation. In a turbulent flow computation, this numerical viscosity may dominate the original viscosity ν, causing the effective Reynolds number in the computation to be smaller than $Re = \nu^{-1}$. Using the cG(1)cG(1)-method, we have an anisotropic visosity term of the type $\nu_{ij} = \delta(U_h)_i(U_h)_j$, and if we use artificial viscosity we have an additional isotropic viscosity of the type $\nu_{av} = \kappa_3|R(U_h, P_h)|h^2$, with $R(U_h, P_h)$ defined by (2.12). If we use artificial viscosity the effective viscosity in the computation is the sum $\nu + \nu_{av}$, and if ν is dominated by ν_{av}, the effective viscosity is independent of the choice of ν. If we on the other hand do not use artificial viscosity, the numerical viscosity is anisotropic and not trivially coupled to ν. The question is if also in this case the solution is independent of the choice of ν, for ν below a certain limit, and if so, where is this limit corresponding to the effective numerical isotropic viscosity? We now present a test where we have used an initial solution from the test example in Section 4 at $t = 20$, and we solve using the cG(1)cG(1)-method for different ν. We present the L_2-norm of $\partial U_1/\partial x_1$ and $\partial U_1/\partial x_2$ in Fig.9, for different ν. We find that for $\nu^{-1} < 100000$, the flow is not independent of ν. It is hard to relate the anisotropic numerical viscosity to an effective Reynolds number Re_{eff}, but a rough estimate may be $Re_{eff}^{-1} \approx \delta|\bar{U}_h|^2$, with $\bar{U}_h$ a mean value of U_h, which would give $Re_{eff} \approx 1000$ in the computations in this paper with $h = 1/64$.

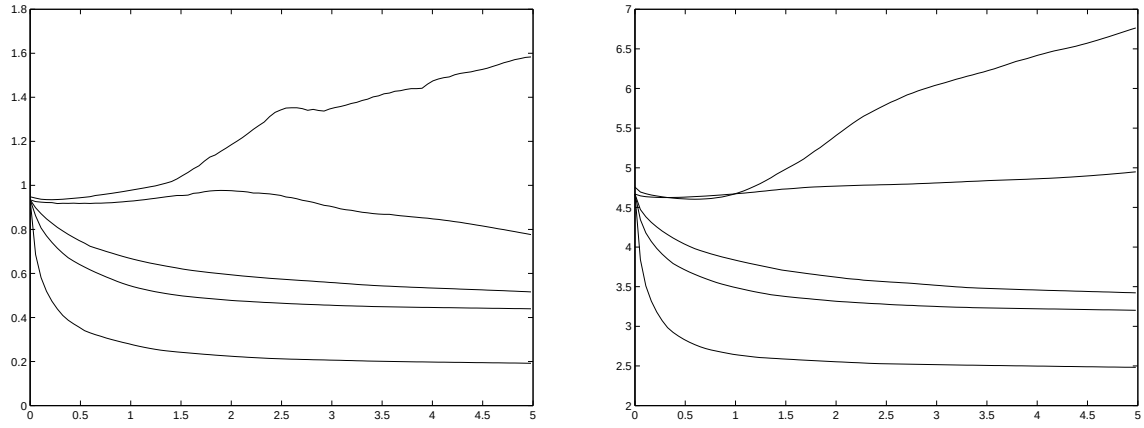

FIGURE 9. $\|\partial U_1/\partial x_1\|$ (left) and $\|\partial U_1/\partial x_2\|$ (right), for $\nu^{-1} = 100, 500, 1000, 10000, 100000$

5. Adaptive strategies for turbulent flow computations

In this paper we have outlined methods to evaluate the errors in a turbulent flow computation, and there are several possible adaptive strategies in which these methods can be put into work.

Since we may estimate both the discretization error and the modeling error, a possible adaptive strategy is pure mesh refinement, with a refinement criterion based on both the discretization error and the modeling error. In this case we are less sensitive to the quality of the subgrid model, since we only need to estimate the size of the modeling error using a subgrid model.

We may include a subgrid model in the adaptive algorithm, since we have methods for estimating both the discretization error and the modeling error also for this case. The refinement criterion is based on both the discretization error and the modeling error, and we may also include the possibility to test different subgrid models to find the best one for the particular problem.

References

[1] J.Bardina, J.H.Ferziger, W.C.Reynolds. Improved subgrid model for large-eddy simulation. *AIAA paper 80-1357*, 1980.

[2] K. Eriksson, D. Estep, P. Hansbo and C. Johnson. Introduction to Adaptive Methods for Differential Equations. Acta Numerica, pp 105–158, 1995.

[3] K. Eriksson, D. Estep, P. Hansbo and C. Johnson. *Computational Differential Equations*, Cambridge University Press, 1996.

[4] U. Frisch. *Turbulence - The Legacy of A. N. Kolmogorov*, Cambridge Univ. Press, 1995.

[5] T.B Gatski, M. Y. Hussaini and J.L. Lumley. *Simulation and Modeling of Turbulent Flow*, Oxford Univ. Press, 1996.

[6] M.Germano, U.Poimelli, P.Moin and W.Cabot. A dynamic subgrid scale eddy-viscosity model. Phys. Fluids A 3, 1760, 1991.
[7] J. Hoffman, C. Johnson and S. Bertoluzza. Dynamic Subgrid Modeling I. Preprint. Chalmers Finite Element Center, to appear in *Comp. Meth. Appl. Mech. Eng.*, 1999
[8] J. Hoffman. Dynamic Subgrid Modeling II. Preprint Chalmers Finite Element Center, 2000.
[9] J. Hoffman. Dynamic Subgrid Modeling for Convection-Diffusion Equations with Fractal Coefficients. *Multiscale and Multiresolution Methods*, Lecture Notes in Science and Engineering, **20**, Springer Verlag, 2001.
[10] J. Hoffman. Dynamic Subgrid Modeling for Convection-Diffusion-Reaction Systems with Fractal solutions. to appear in *International Journal for Numerical Methods in Fluids*, 2001.
[11] J.Hoffman and C.Johnson. Adaptive finite element methods for incompressible fluid flow. *2001 NATO-RTO Lecture Series*, Springer Lecture Series, Springer Verlag, 2002.
[12] J.Hoffman and C.Johnson. A computational study of transition to turbulence in shear flow. *Chalmers finite element center, preprint 2002-04*, 2002.
[13] J.Hoffman. Adaptive finite element methods for turbulent flow. *Chalmers finite element center, preprint*, 2002.
[14] T.J.R.Hughes, L.Mazzei, K.E.Jansen. Large Eddy Simulation and the variational multiscale method. *Computing and Visualization in Science, **3**, 47-59*, 2000.
[15] M.Lesieur. *Turbulence in Fluids.* Kluwer Academic Publishers, London, England, 1997.
[16] S.Liu, C.Meneveau, J.Katz. On the properties of similarity subgrid-scale models as deduced from measurements in turbulent jet. *J. Fluid Mech., **275**, 83-119*, 1994.
[17] G.Papanicolau, K.Solna. Wavelet based estimation of local Kolmogorov turbulence. *Long-range Dependence Theory and Applications.* Birkhauser, 2001.
[18] R. Rannacher. Finite element methods for the incompressible Navier Stokes equations, Preprint Intsitute of Applied Mathematics, Univ. of Heidelberg, 1999.
[19] A.Scotti, C.Meneveau. Fractal dimension of velocity signal in high-Reynolds-number hydrodynamic turbulence. *Phys. Review E **51**, 5594*, 1995.

Chalmers Finite Element Center Preprints

2001–01 *A simple nonconforming bilinear element for the elasticity problem*
Peter Hansbo and Mats G. Larson

2001–02 *The $\mathcal{LL}^*$ finite element method and multigrid for the magnetostatic problem*
Rickard Bergström, Mats G. Larson, and Klas Samuelsson

2001–03 *The Fokker-Planck operator as an asymptotic limit in anisotropic media*
Mohammad Asadzadeh

2001–04 *A posteriori error estimation of functionals in elliptic problems: experiments*
Mats G. Larson and A. Jonas Niklasson

2001–05 *A note on energy conservation for Hamiltonian systems using continuous time finite elements*
Peter Hansbo

2001–06 *Stationary level set method for modelling sharp interfaces in groundwater flow*
Nahidh Sharif and Nils-Erik Wiberg

2001–07 *Integration methods for the calculation of the magnetostatic field due to coils*
Marzia Fontana

2001–08 *Adaptive finite element computation of 3D magnetostatic problems in potential formulation*
Marzia Fontana

2001–09 *Multi-adaptive galerkin methods for ODEs I: theory & algorithms*
Anders Logg

2001–10 *Multi-adaptive galerkin methods for ODEs II: applications*
Anders Logg

2001–11 *Energy norm a posteriori error estimation for discontinuous Galerkin methods*
Roland Becker, Peter Hansbo, and Mats G. Larson

2001–12 *Analysis of a family of discontinuous Galerkin methods for elliptic problems: the one dimensional case*
Mats G. Larson and A. Jonas Niklasson

2001–13 *Analysis of a nonsymmetric discontinuous Galerkin method for elliptic problems: stability and energy error estimates*
Mats G. Larson and A. Jonas Niklasson

2001–14 *A hybrid method for the wave equation*
Larisa Beilina, Klas Samuelsson and Krister Åhlander

2001–15 *A finite element method for domain decomposition with non-matching grids*
Roland Becker, Peter Hansbo and Rolf Stenberg

2001–16 *Application of stable FEM-FDTD hybrid to scattering problems*
Thomas Rylander and Anders Bondeson

2001–17 *Eddy current computations using adaptive grids and edge elements*
Y. Q. Liu, A. Bondeson, R. Bergström, C. Johnson, M. G. Larson, and K. Samuelsson

2001–18 *Adaptive finite element methods for incompressible fluid flow*
Johan Hoffman and Claes Johnson

2001–19 *Dynamic subgrid modeling for time dependent convection–diffusion–reaction equations with fractal solutions*
Johan Hoffman

2001–20 *Topics in adaptive computational methods for differential equations*
Claes Johnson, Johan Hoffman and Anders Logg

2001–21 *An unfitted finite element method for elliptic interface problems*
Anita Hansbo and Peter Hansbo

2001–22 *A P^2–continuous, P^1–discontinuous finite element method for the Mindlin-Reissner plate model*
Peter Hansbo and Mats G. Larson

2002–01 *Approximation of time derivatives for parabolic equations in Banach space: constant time steps*
Yubin Yan

2002–02 *Approximation of time derivatives for parabolic equations in Banach space: variable time steps*
Yubin Yan

2002–03 *Stability of explicit-implicit hybrid time-stepping schemes for Maxwell's equations*
Thomas Rylander and Anders Bondeson

2002–04 *A computational study of transition to turbulence in shear flow*
Johan Hoffman and Claes Johnson

2002–05 *Adaptive hybrid FEM/FDM methods for inverse scattering problems*
Larisa Beilina

2002–06 *DOLFIN - Dynamic Object oriented Library for FINite element computation*
Johan Hoffman and Anders Logg

2002–07 *Explicit time-stepping for stiff ODEs*
Kenneth Eriksson, Claes Johnson and Anders Logg

2002–08 *Adaptive finite element methods for turbulent flow*
Johan Hoffman

These preprints can be obtained from

`www.phi.chalmers.se/preprints`